Schweizerische Eidgenossenschaft
Confédération suisse
Confederazione Svizzera
Confederaziun svizra

Department of the Environment, Transport, Energy and Communication DETEC

Swiss Federal Office of Energy SFOE
Energy Research

Final report

Highly efficient CIGS solar cells

On the road towards 25% efficiency

Empa
Materials Science and Technology

Date: 01.10.2017
Town: Dübendorf

Publisher:
Swiss Federal Office of Energy SFOE
Photovoltaic Research Programme
CH-3003 Bern
www.bfe.admin.ch

Co-financed by:
This work received additional support from the Swiss State Secretariat for Education, Research and Innovation under contract number 15.0158.

Agent:
Laboratory for Thin Films and Photovoltaics, Empa
Überlandstr. 129
CH-8600 Dübendorf
www.empa.ch

Author:
J. Löckinger, Empa, Laboratory for Thin Films and Photovoltaics, Johannes.loeckinger@empa.ch
B. Bissig, Empa, Laboratory for Thin Films and Photovoltaics, Benjamin.bissig@empa.ch
S. Buecheler, Empa, Laboratory for Thin Films and Photovoltaics, Stephan.buecheler@empa.ch
A. N. Tiwari, Empa, Laboratory for Thin Films and Photovoltaics, Ayodhya.tiwari@empa.ch

SFOE head of domain: Dr. Stefan Oberholzer, stefan.oberholzer@bfe.admin.ch
SFOE programme manager: Dr. Stefan Nowak, Stefan.nowak@netenergy.ch
SFOE contract number: SI/501145-01

Swiss Federal Office of Energy SFOE
Mühlestrasse 4, CH-3063 Ittigen; postal address: CH-3003 Bern
Phone +41 58 462 56 11 · Fax +41 58 463 25 00 · contact@bfe.admin.ch · www.bfe.admin.ch

Contents

List of abbreviations

ALD	Atomic layer deposition
CBD	Chemical bath deposition
CGI	Copper concentration versus Indium and Gallium concentration in the Cu(In,Ga)Se_2 material
CIGS	Cu(In,Ga)Se_2, compound semiconductor used as absorber in thin film solar cells
CV	capacitance voltage
EBIC	Electron beam induced current
EQE	External quantum efficiency
FF	Fill factor
FFT	Fast _Fourier transform
GGI	Gallium concentration versus Indium and Gallium concentration in the Cu(In,Ga)Se2 material
IV	Current voltage characteristics
Jsc	Short circuit current density
KIS	Compound consisting of Potassium, Indium and Selenium
MIS-structure	Metal insulator semiconductor structure
NIR	Near infrared region
PDT	post deposition treatment
PEALD	Plasma enhanced atomic layer deposition
pl	Passivation layer
PV	Photovoltaic
QE	Quantum efficiency
SEM	Scanning electron microscope
SLG	Soda lime glass
TCAD	Technology computer-aided design
TDMAH	Tetrakis(dimethylamido)hafnium
TDMAT	Tetrakis(dimethylamido)titanium
TEM	Transmission electron microscope
TMA	Trimethylaluminium
TMM	Transfer matrix method
TRPL	Time resolved photoluminescence
TU	Thiourea
Voc	Open circuit voltage

Zusammenfassung

Das Ziel des Projektes war es noch existierende Verluste in $Cu(In,Ga)Se_2$ basierten Dünnschichtsolarzellen aufzudecken und Strategien zu entwickeln, wie der Wirkungsgrad solcher Solarzellen auf 25% erhöht werden kann. Hierbei wurden neu Wege erforscht, Verluste an Grenzflächen mittels Feld Effekt und/oder chemischer Passivierung zu minimieren. Des Weiteren wurde die Zusammensetzung und Herstellungsverfahren des Verbindungshalbleiters $Cu(In,Ga)Se_2$ hinterfragt. Im Rahmen des Projektes wurden Konzepte zur Erhöhung des Photostroms ausgearbeitet und umgesetzt. Die hierbei gefundenen Prozesse zeigen eine noch höhere Reproduzierbarkeit bei gleichzeitig höherem Durchschnittswirkungsgrad.

Résumé

Le projet vise au développement de nouvelles stratégies de réduction des recombinaisons non-radiatives dans les cellules solaires $Cu(In,Ga)Se_2$, afin d'en améliorer les paramètres photovoltaïques en vue d'atteindre 25% d'efficacité énergétique. Pour ce faire de nouvelles stratégies ont été explorées afin de passiver le matériau et en particulier les interfaces. Des procédés de points de contacts ont été explorés, et des oxydes métalliques déposés par dépôt de couches atomiques ont été étudiés en tant que matériaux de passivation. La composition et les conditions de déposition des absorbeurs $Cu(In,Ga)Se_2$ ont été revues et optimisées, résultant en un gain de photocourant dû à une meilleure absorption. Les procédés développés s'avèrent plus robustes et permettent d'améliorer l'efficacité énergétique moyenne.

Summary

The project aimed for development of novel strategies to reduce non radiative recombination mechanism in order to improve the photovoltaic parameters in $Cu(In,Ga)Se_2$ solar cells towards 25% power conversion efficiency. To do so, novel passivation strategies for bulk and especially interfaces have been explored. Point contacting schemes were explored and metal oxides deposited from atomic layer deposition were investigated as passivating materials. The composition and deposition conditions for the $Cu(In,Ga)Se_2$ absorber have been revisited and optimized to yield a higher photocurrent by improving the absorption. The developed processes are more robust and yield solar cells with higher average efficiency.

Appendix

No appendix

1 Project goals

Solar cells based on Cu(In,Ga)Se_2 absorber layers have shown highest energy conversion efficiency of 22.6% [2] among all polycrystalline photovoltaic (PV) technologies. The most relevant path to strengthen the industrial competiveness of the CIGS technology comes with further efficiency improvement. After nearly one decade of mostly incremental increase the introduction of a so called alkaline fluoride post deposition treatments (PDTs) has led to a series of new records for various types of buffer layers and deposition approaches [2] [3] [4]. A widening of the absorber composition window that allows high efficiencies was shown, which motivates to revisit high bandgap or copper content approaches [5]. Furthermore, the importance of surface/interface related effects of the alkaline PDT was indicated [1] [6-9], suggesting further improvement of the hetero-interface as a route towards higher efficiencies. Therefore front and back contact passivation concepts will be explored in terms of this project. Approaches such as partial surface passivation in Si technology [10] [11] have recently been successfully introduced at the back contact of thin CIGS solar cells [12]. The implementations of similar concepts for highly efficient devices - where diffusion lengths are expected to be high - are one of the goals of this project.
This requires in-depth experimental as well as theoretical analysis of potential candidates (e.g. Al_2O_3, HfO_2, TiO_2) as well as experimental tools to produce these layers e.g. by atomic layer deposition (ALD) and to characterize their effectiveness e.g. by time-resolved photoluminescence (TRPL).
Apart from losses due to diode non-idealities the near infrared current loss (>700 nm) is another limiting factor in state of the art CIGS devices, especially as compared to other thin film technologies such as CdTe. Short carrier collection length and/or incomplete absorption can be responsible for such losses. First of which can be addressed by exploring other absorber compositions aiming to reduce point defect density, band gap or potential fluctuations. The latter can be approached by optimization of bandgap profile guided by simulation. The overall goal is a comprehensive understanding of these various effects and especially their relation deposition process parameters in order to derive novel process approaches.

The primary objective of this project was to push the efficiency of CIGS closer to the theoretical limits and to understand fundamental limitations of state of the art devices. Specifically, the individual objectives are:

- Improve the collection of charge carriers generated by photons in the wavelength region from 700 nm to 1100 nm resulting in additional photocurrent density of at least 1.0 mA/cm^2
- Introduce a novel CIGS surface passivation process to reduce interface recombination. Together with further improvement of the CIGS bulk properties an improvement in V_{OC} (+ 30 to 50 mV) and FF (+ 1% to 2% absolute) is expected
- Reduce parasitic absorption in the buffer layer to increase J_{SC} by 0.5 to 1.0 mA/cm^2
- Develop robust deposition processes to improve the average lab cell efficiency from currently around 17%-18% to above 20% and highest record efficiency to 22%
- Define a roadmap from 22% towards 25% efficiency

2 Completed tasks and achieved results

2.1 Task 1: Revisit CIGS absorber deposition & role of alkaline elements

2.1.1 Find optimum CIGS deposition

In order to more precisely control the amount of Se evaporated in the CIGS absorber layer deposition process, which is paramount for reproducibility, a flux monitor system by MBE Komponenten was installed (see Figure 1).

Figure 1: Photograph of the Flux-Monitor installed on the evaporation chamber and the GUI shown on the right.

The current losses observed in the near infrared spectral region of quantum efficiency measurements in CIGS solar cells originate from incomplete optical absorption or poor collection of photo generated charge carriers. To discriminate between the contributions electron beam induced current (EBIC) measurements were performed on device cross-sections [13]. By this approach depth resolved information about the charge carrier collection probability is accessible. An ALD-Al_2O_3 layer was found to be necessary to reduce surface recombination at the cleaved cross-section to more accurately determine the collection efficiency. From EBIC measurements the expected quantum efficiency was calculated and compared with the direct measurements (Figure 2). The minority carrier collection probability is found to be >75% up to 1.6 µm from the CdS/CIGS interface. Compared to the case of ideal collection, the residual current loss due to insufficient collection is estimated to be about 0.2 mA cm^{-2}. The residual NIR EQE losses as compared to the total absorption limit can be calculated to be around 2 mA cm^{-2} and consequently are assumed to be due to insufficient absorption. This clearly motivates approaches to increase the NIR response and hence Jsc by improving the absorption in the CIGS layer. Strategies include increasing the thickness of the low band gap region and the absorption coefficient at the band gap.

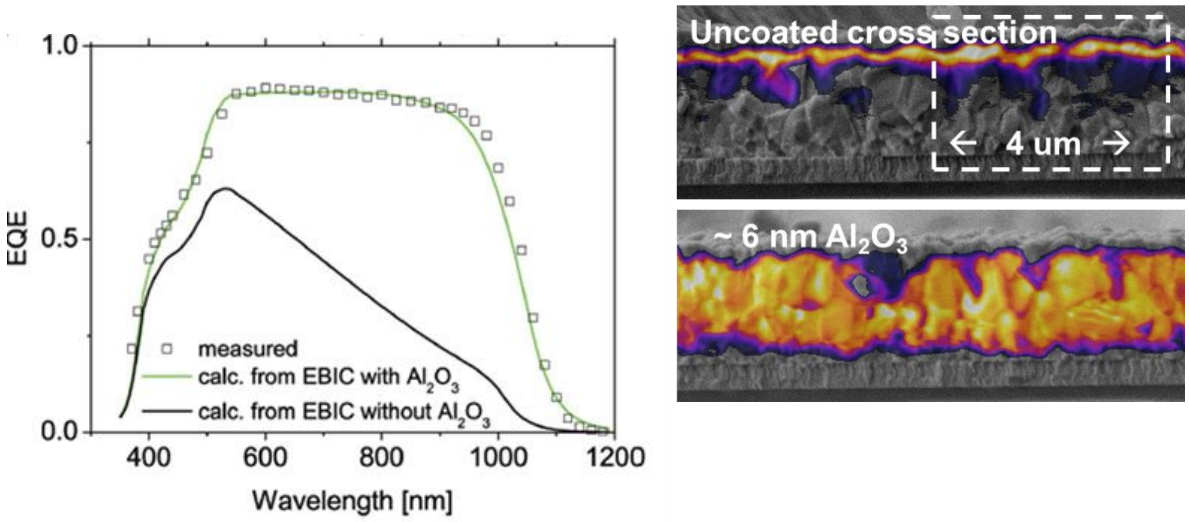

Figure 2: left: Measured (squares) and calculated (lines) EQE for a CIGS device based on EBIC measurements (shown on the right) with (green) and without (black) Al_2O_3 coated cross-section. right: SEM of a cross-section of a CIGS device with the EBIC signal overlaid. The uncoated surface shows a limited collection width which would result in a much reduced EQE. The by Al_2O_3 passivated surface gives a more accurate EBIC measurement from which the measured EQE could be closely reproduced.

2.1.2 Approaches for increased NIR absorbance – Increased thickness and notch widths

The in-situ Se flux control system allowed for a precise control of the [Se]/([metal] flux ratio during the CIGS deposition. It was found that the [Ga]/([In]+[Ga]) (GGI) grading is different if the low temperature multistage process for CIGS growth is conducted under low ([Se]/([Cu]+[Ga]) = 2.5) or high ([Se]/([Cu]+[Ga]) = 7.5) conditions. The steepness of the grading and the GGI notch width, i.e. region of minimum bandgap, could be controlled by optimizing the Se flux especially during the 2nd stage of deposition. With a similar shape of the GGI grading but an increased notch width and thickness of the CIGS absorber the Jsc could be increased from typical 33 to over 35 mA cm^{-2} without anti-reflective coating [14]. The improvement of the quantum efficiency and the evolvement of the Jsc with CIGS thickness are depicted in Figure *3*.

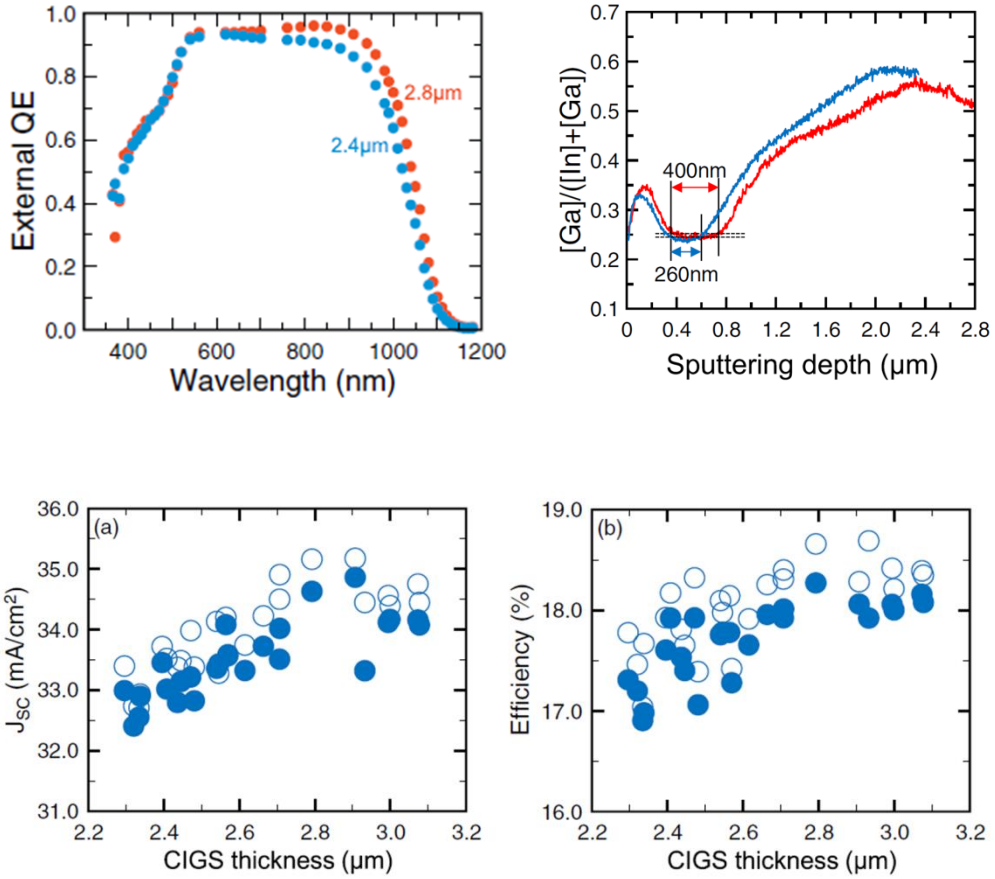

Figure 3: above: EQE of devices with different CIGS layer thickness grown in a Se flux of [Se]/([Cu]+[Ga]) ~4 and corresponding GGI grading determined from SIMS measurements. below: CIGS thickness dependence of Jsc (a) and efficiency (b), closed and open circles indicate average and best results on one substrate, respectively. Only NaF PDT was applied. Increasing the CIGS thickness and notch width leads to an improved Jsc and efficiency with an optimum at about 3 µm.

2.1.3 Approaches for increased NIR absorbance – Cu content variations

In a further study the influence of the [Cu]/([In]+[Ga]) (CGI) ratio in CIGS absorber layers on the absorption behaviour was investigated [15]. Keeping the thickness constant but increasing the copper content improves the absorption in the NIR region which is reflected in the EQE measurement shown in Figure 4. All samples are still Cu-poor and have a similar GGI at the CIGS/CdS interface. The improved NIR-EQE is ascribed to an improved optical effect rather than to charge carrier collection effects. The CGI was increased by up to 18% as compared to the reference (CGI 0.79). It was found that the first CGI increase of 8% is responsible for the improved NIR-EQE. In order to separate the effects of the different bandgap gradings, i.e. the lower minimum bandgap for the reference case, from the influence of the Cu content transfer matrix method (TMM) simulations were performed. The simulations suggest that the observed gain is rather due to the difference in CGI than GGI grading. The observation can be explained, as it was shown that material of increased CGI features higher absorption coefficients in the region close to the bandgap [17].

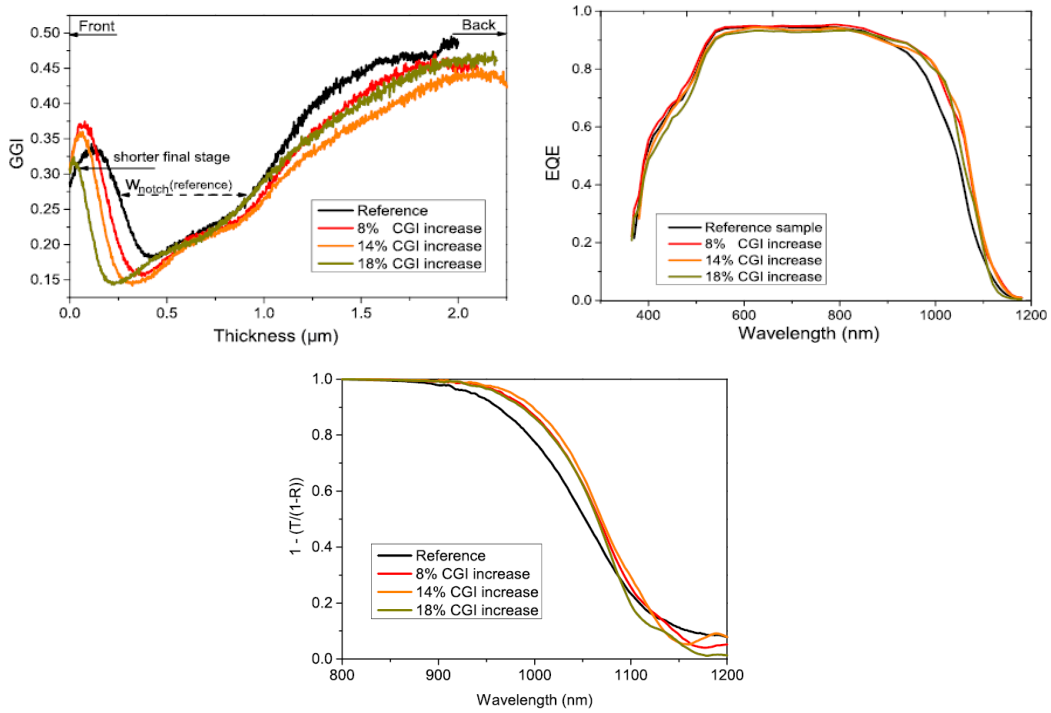

Figure 4: *a) GGI grading b) EQE spectra and c) optical absorption spectra of CIGS devices with increasing CGI and GGI notch width. A gain in absorption is visible for a 8% CGI increase when compared to a reference with a CGI of 0.79 which is leading to an improved EQE in the NIR region.*

2.1.4 Influence of alkali PDT

In TRPL measurements the luminescent decay intensity of an optically excited semiconductor is tracked as a function of time. In general, the decay rate is governed by different mechanisms such as carrier drift, diffusion, trapping and different paths of recombination (radiative, bulk defect related or surface related). Thus, the technique can theoretically be used to study these processes and parameterize absorber quality.

In *Figure 5* the slow decay times extracted from TRPL measurements as function of excitation level for samples coated with CdS are presented for CIGS cells with various PDT. In both series one sample did not undergo a PDT, the second sample had NaF and the third NaF+KF or NaF+RbF PDT, respectively. The decays were measured at different excitation levels. For both series, the samples without PDT show significantly faster decay times. In the case when a PDT was performed, either NaF only or NaF + heavy alkali PDT, no significant difference in the slow decay time was observed over a wide range of excitation levels. No correlation between the decay time and the observed increase of V_{OC} by 30 meV in the I-V characteristics was found when comparing the NaF only and the NaF + KF samples.

If the measured low excitation decay times are interpreted as actual bulk minority carrier lifetimes this would indicate excellent crystal quality as the corresponding non-radiative recombination rate approaches the radiative rate that was estimated to be about 1 μs^{-1}. However, no conclusive explanation was given yet for the decrease in decay time towards higher injection levels. Also, a more detailed investigation of the effects of grading, trapping and surface- recombination and fields will be

necessary to more quantitatively characterize bulk lifetimes of bandgap graded and surface treated absorbers.

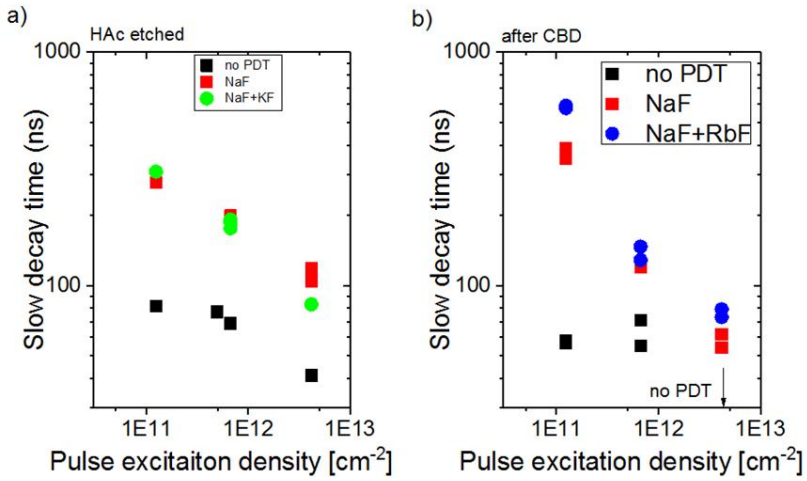

Figure 5: TRPL slow decay times measured on CIGS samples with various alkali PDT (no PDT, NaF only and a) NaF+KF or b) NaF+RbF PDT) coated with CdS. Samples without PDT show significantly faster decay times. In the case when a PDT was performed, either NaF only or NaF + heavy alkali PDT, no significant difference in the slow decay time was observed over a wide range of excitation levels. A decrease in decay time for higher injection levels, i.e. pulse excitation density, for all samples was observed.

2.2 Task 2: CIGS surface passivation & junction formation

Development of TRPL methodology:
A measurement system to perform TRPL was installed at Empa. A commercially available tool (FT300) from PicoQuant was extended to allow measurements at well controlled experimental conditions in case of thin film material (see *Figure* ***6***). The setup is equipped with three different picosecond lasers to excite materials at different wavelengths (400 nm, 640 nm, 980 nm). Spectrally resolved measurements can be performed in a broad wavelength range from 300 nm to 1400 nm.

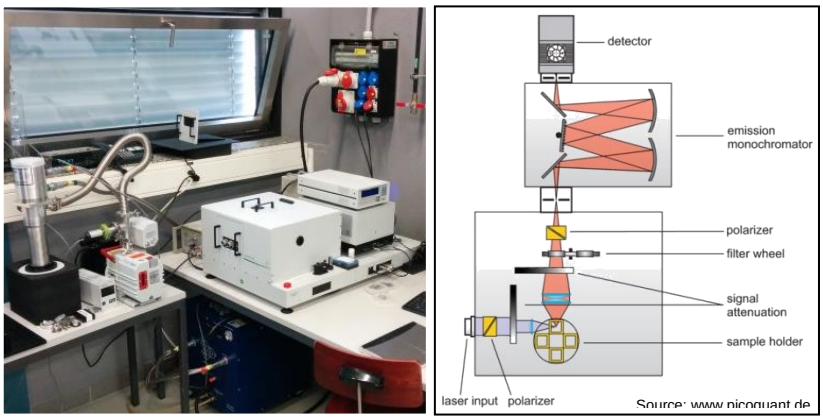

Figure 6: Left: Photograph of the new TRPL system at Empa. Right: Schematic drawing of the system (source: www.picoquant.de).

TRPL and capacitance voltage (CV) studies were performed to assess the effectivity of Al_2O_3 and HfO_2 for their field- or chemical passivation behaviour. The CIGS absorber used in these studies was without intentional bandgap grading and only NaF PDT was applied. The luminescence transients of the absorber in its bare (uncoated, as deposited) and oxide-coated state were compared. TRPL is sensitive to surface modifications, because the surface states lead to additional recombination in addition to the bulk. Thus it can be expected that a passivated surface i.e. a reduced surface recombination rate leads to increased TRPL decay time as compared to a more defective surface. TRPL transients were recorded with a pulse photon excitation of ~ 6.7e11 cm^{-2} $pulse^{-1}$ (close to low injection) with a repetition rate of 1 MHz and a laser wavelength of 639 nm (~100 nm absorption depth). The measured luminescent yield showed a rapid decrease during the first ~10 ns followed by a mono-exponential decay from which the reported lifetimes were extracted. *Figure 7* shows a typical measurement with the fitting procedure applied to extract the decay time. The dependency of this decay on the thickness and deposition temperature of the oxide layer is shown in *Figure 8*.

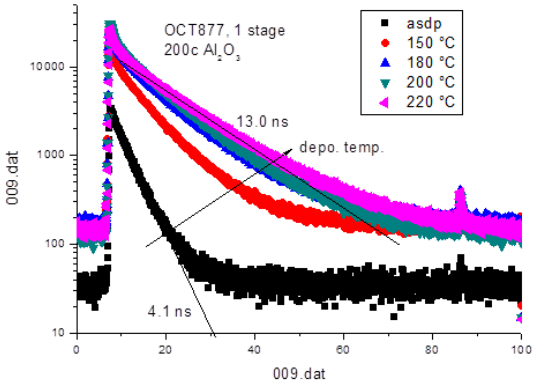

Figure 7: TRPL spectra of a CIGS device coated with Al_2O_3 at different deposition temperatures as compared to the bare absorber layer (asdp). Increased decay times are observed when the deposition temperature of ALD-Al_2O_3 is increased.

It can be seen that by increasing the thickness of the oxides from about 5 to 10 nm and the deposition temperature from 150 to 200°C the measured decay times increase and saturate. In comparison, for the case of fresh and uncoated samples decay times around 25 ns or partially somewhat higher were measured. In contrast to the stable oxide coated samples, for the uncoated samples the decay times were observed to decrease within hours to days upon storage rapidly towards only few ns. By TRPL measurements no significant difference between Al_2O_3 and HfO_2 was observed. Both oxides seem to stabilize the absorber surface showing a similar recombination activity as a fresh, uncoated surface. This observation shows the potential of alumina or hafnia to reduce the surface recombination as compared to the bare CIGS surface.

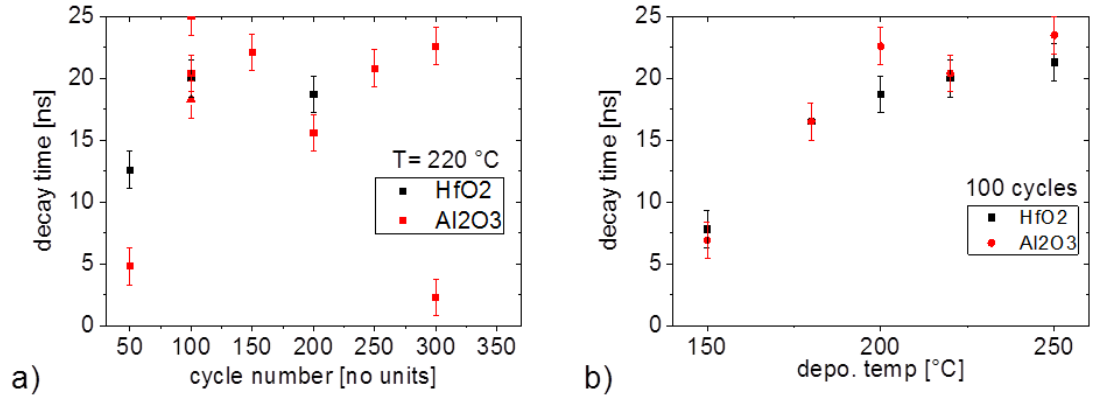

Figure 8: Luminescent decay times derived by TRPL measurements as a function of thickness and deposition temperature for HfO_2 and Al_2O_3 on an ungraded CIGS absorber. The measured decay times increase and saturate when increasing the thickness of the oxides from about 5 to 10 nm and the deposition temperature from 150 to 200°C.

CV measurements were performed on metal-oxide-semiconductor/back-contact devices (MIS structure, in this case: Mo/CIGS/oxide/Al) to determine the fixed charge densities in the vicinity of the oxide-semiconductor interface. Al_2O_3 and HfO_2 oxides were deposited at 220°C at various thicknesses and with different surface treatments before ALD on CIGS which was again deposited in a single stage process. The sample showed pronounced hysteresis effects i.e. the forward and backward measurements do not coincide. Furthermore, the width of the hysteresis loop is found to scale with the maximally applied voltage. This behavior deviates significantly from the model case and therefore does not allow straightforward quantification of the fixed charge. Possible explanations for the shift in transition voltage could be charging of slow oxide defects, for instance by charge tunneling into the oxide layer upon bias. Also, biasing could lead to formation of additional, charged interface defects leading to modified electrostatics. Similar behavior was observed for HfO_2 and Al_2O_3 at various layer thicknesses. Concluding from this observation it was not possible to extract parameters such as fixed charge densities or interface defect densities by capacitance based measurements. Understanding and minimizing the hysteretic effects in our devices would allow parameterizing the passivating behavior of oxides on CIGS and give more insights in the necessity of including them into the device architecture as alternative buffer layer.

2.2.1 Development of alkali templated surface nano-patterning approach for CIGS

Testing the passivating properties of Al_2O_3 or HfO_2 in a CIGS device requires a method to structure the oxide layers due to their high resistivity. The required distance and diameter of point contacts through passivating dielectrics on front and backside were estimated to be on the sub-micrometre range [1].

In order to estimate the projected device improvement upon application of front surface passivation 2D simulations on TCAD environment were performed [1]. Starting point was an interface recombination limited device without front contact passivation showing intermediate Voc and FF (~ 650 mV, 55%). Then a passivation layer (pl) in the sense that the pl/CIGS interface was defect free and featuring a conduction band offset of 0.5 eV was introduced in the device structure. Furthermore point contacts through the passivation layer were defined at distances of 50 nm, 100 nm, and 250 nm. Finally, the point contact diameter was used as parameter to study the effect of the passivation layer on Voc and FF.

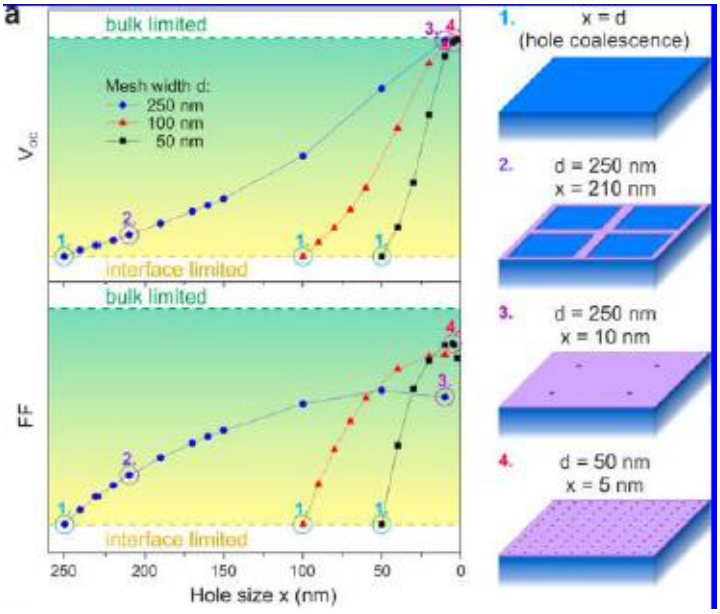

Figure 9: Simulated Voc and FF in dependence of surface passivation geometry. The CIGS(blue)/passivation-layer(purple) interface is set to be defect free and transport through the passivation layer is inhibited by 0.5 eV conduction band offset. With decreasing point contact size Voc and FF are increasing, if surface coverage ratio gets too high parasitic resistive effects reduce the FF.

The right hand side in *Figure 9* visualizes a variety of surface coverage geometries. Corresponding simulations are displayed on the left hand side. It can be seen that Voc and FF generally increase upon reduction of point contact size i.e. increase of the passivated surface ratio. Towards full coverage all devices reach open circuit voltages corresponding to an interface defect free case that is limited by bulk recombination only. On the other hand, for highest coverage ratios a significant decrease in FF is observed. It can be explained by the decreased diode conductivity due to the increased resistance through the point contacts. This effect is strongly dependent on point contact difference and the simulation makes clear, that only front contact structuring on the intermediate nm scale will allow avoiding resistive losses. This underlines the necessity of well-defined passivation layer deposition schemes.

The approach that we developed is the use of a surface nano-pattern as obtained for certain PDT parameters. *Figure 10* displays a top view SEM micrograph of the absorber surface after NaF and KF PDT. Prior to imaging the samples were rinsed in H_2O as shown in the schematics on the right hand side. Before rinsing, cubic alkali crystals are clearly visible on the surface. The crystals are embedded into a non-CIGS surface layer which was shown to be composed of K-In-Se (KIS) and to be Cu free [9] [1]. If etched in HCl this surface layer is removed. The nano-structuring approach then consists of the deposition of a passivating dielectric prior to water rinsing. In the rinsing step, the dielectric is then partially removed together with the salt. The remaining dielectric is punctuated with opening to the underlying absorber. In a preliminary experiment the approach was shown to work for patterning of

sputtered gold coatings. Notably, as discussed below, already the KIS surface layer itself is believed to have interface passivating properties.

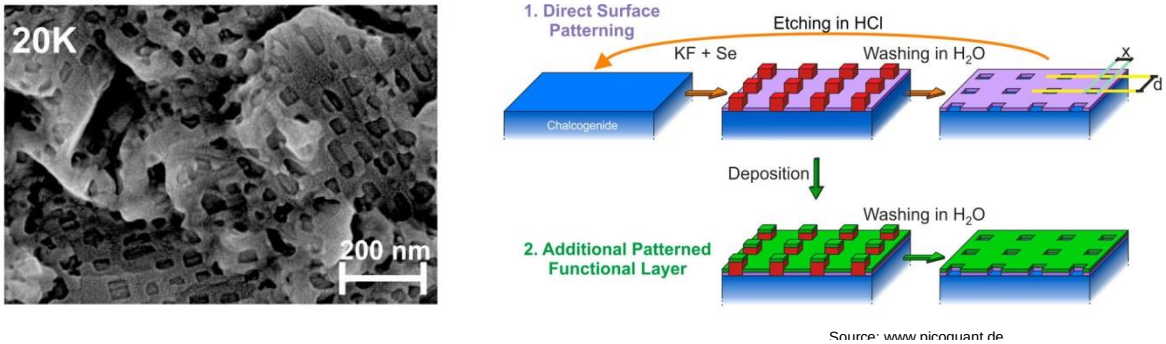

Figure 10: Left: SEM image of absorber surface in case of 20 min NaF PDT followed by 20 min KF PDT at 350 °C after a H_2O rinse. A nanopatterned K-In-Se containing surface layer is visible. The nanopatterning is due to removal of alkali crystals upon rinsing. Right: Sketch of possible approach to exploit the alkali template for deposition of functional layers such as additional passivation layers.

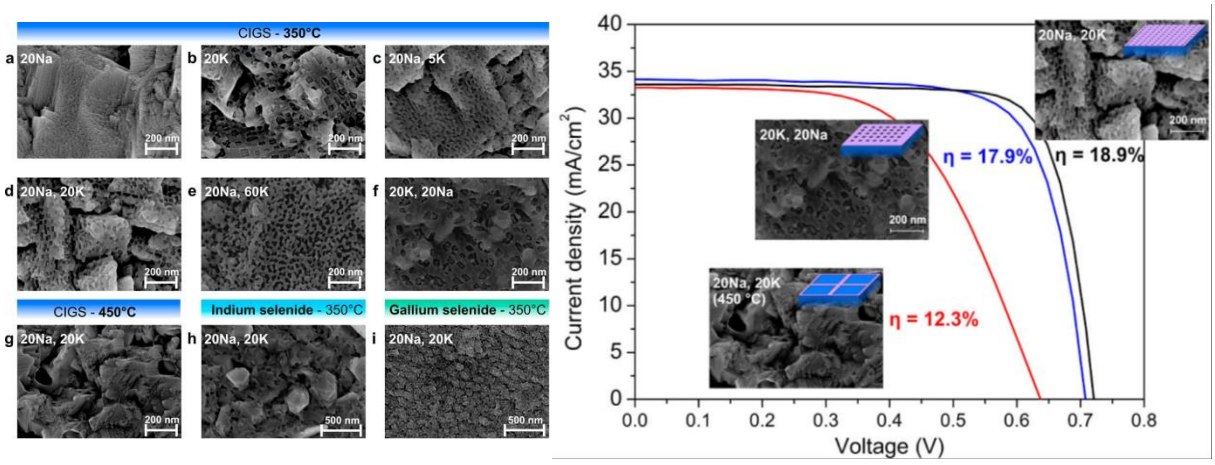

Figure 11: Left: SEM micrographs of CIGS surface for different PDT parameters i.e. NaF/KF time and temperature. Nano pattern geometry can be tuned over wide range of point sizes and distances. Right: IV curves as measured for samples with different surface pattern geometries. SEM micrographs and corresponding geometry schematics are displayed next to the curves. A clear impact of the surface coverage state can be observed.

In order to exploit the effect of surface structure geometry for operating devices, the process parameters of the PDT were varied. Upon changing PDT time, sequence or temperature various surface layer geometries can be achieved. On the left hand side of *Figure 11* a selection of possible patterns is displayed together with the respective NaF and KF times. Notably, the approach works in a similar manner on pure In-Se while on Ga-Se no well-ordered structure is observed, likely due to the lack of In, that is necessary for the formation of a structurable KIS layer.

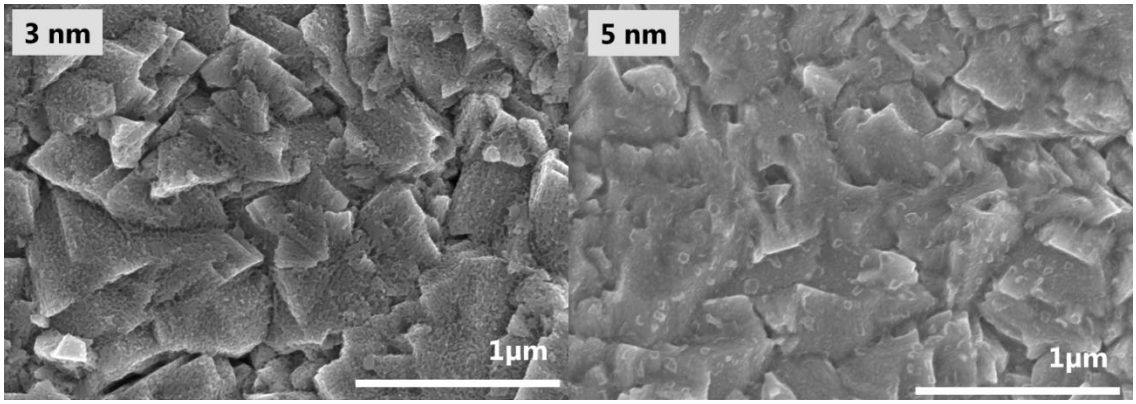

Figure 12: SEM micrographs of 3 or 5 nm HfO2 deposited on CIGS with NaF/KF PDT and subsequent H2O rinse. For 5 nm HfO2 rinsing in water is not effective anymore to pattern the surface.

The right hands side of *Figure 11* shows IV curves, measured on finished devices with different surface preparations. The inlet SEM micrographs and schematics show the corresponding surface coverage distribution. A clear decrease in Voc upon increasing the opening diameter can be observed as predicted from the simulations. Clearly bulk effects cannot be fully excluded, but as thermal budgets and bulk alkali contents are similar in most cases the main change is expected to come from the interface modifications.

The application of this structuring approach was tested for ALD-HfO_2. The major drawback is the limited thickness that can be patterned. In *Figure 12* it can be seen that after a 5 nm thick HfO_2 layer has been deposited, rinsing in water has no effect anymore. This is well below the by TRPL suggested thickness necessary for a meaningful surface passivation. Different approaches like optical- and electron beam lithography are candidates for patterning on such scales with well-defined geometries but are hardly scalable. Deposition of templates like polystyrene or nanoparticles with subsequent dielectric deposition and final stripping/washing of the template structure are less defined but promise higher throughput and could be tested in future work.

2.2.2 Reduction of parasitic absorption in buffer layer for Jsc improvement

An alternative buffer layer approach was taken with Zn(O,S) instead of CdS deposited by chemical bath deposition (CBD). Due to the higher bandgap of about 3.4 eV for a [S]/([S]+[O]) ratio of ~0.85 a higher response in the wavelength region of 360-550 nm was obtained in the quantum efficiency measurement as can be seen in *Figure 13*. The I-V characteristics partially reflect this current gain. A reduced Voc and a metastable light-soaking behavior, which could be reduced to less than a minute, were observed. A new bath chemistry with the use of thioamides instead of thiourea lead to an increased deposition rate [16]. The cell efficiency, however, is inferior to a cell comprising a CdS buffer layer.

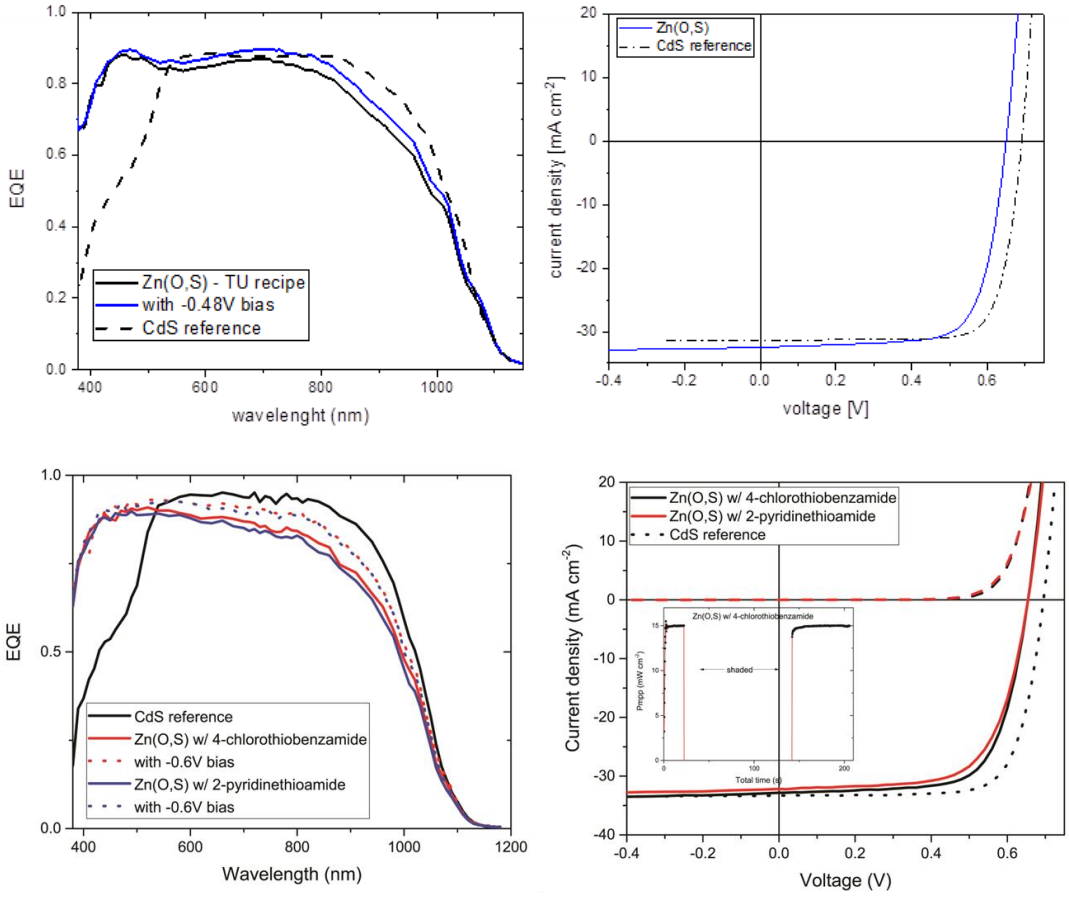

Figure 13: EQE and IV characteristics of a CIGS device with a Zn(O,S) buffer layer deposited from different [S^{2-}] sources (above: thiourea; below: 4-chlorothiobenzamide, 2-pyridinethioamide) compared to a CdS buffer. Similar performance was observed for CIGS devices with Zn(O,S) buffer layer deposited from different [S^{2-}] source.

2.2.3 Introduction of metal oxide based passivation layers

Another approach for increasing Jsc was taken with ALD-TiO_2 as intermediate buffer layer. When reducing the CdS layer thickness, what is usually observed is a severe degradation of the cell performance due to a CIGS/ZnO interface which arises in non-covering areas of CdS on the CIGS surface. Furthermore, the exposure of the CIGS surface to plasma, as is the case in sputtering, showed deteriorating effects. With ALD no plasma damage is imposed and a thinner CdS layer is tolerated. *Figure 14* shows the gain in Jsc due to the reduced CdS layer thickness, while the loss in Voc is negligible. However, the FF is inferior as compared to the reference sample with a thicker CdS and sputtered ZnO buffer layer. Temperature dependent measurements suggest a band-offset at the CdS/TiO_2 interface.

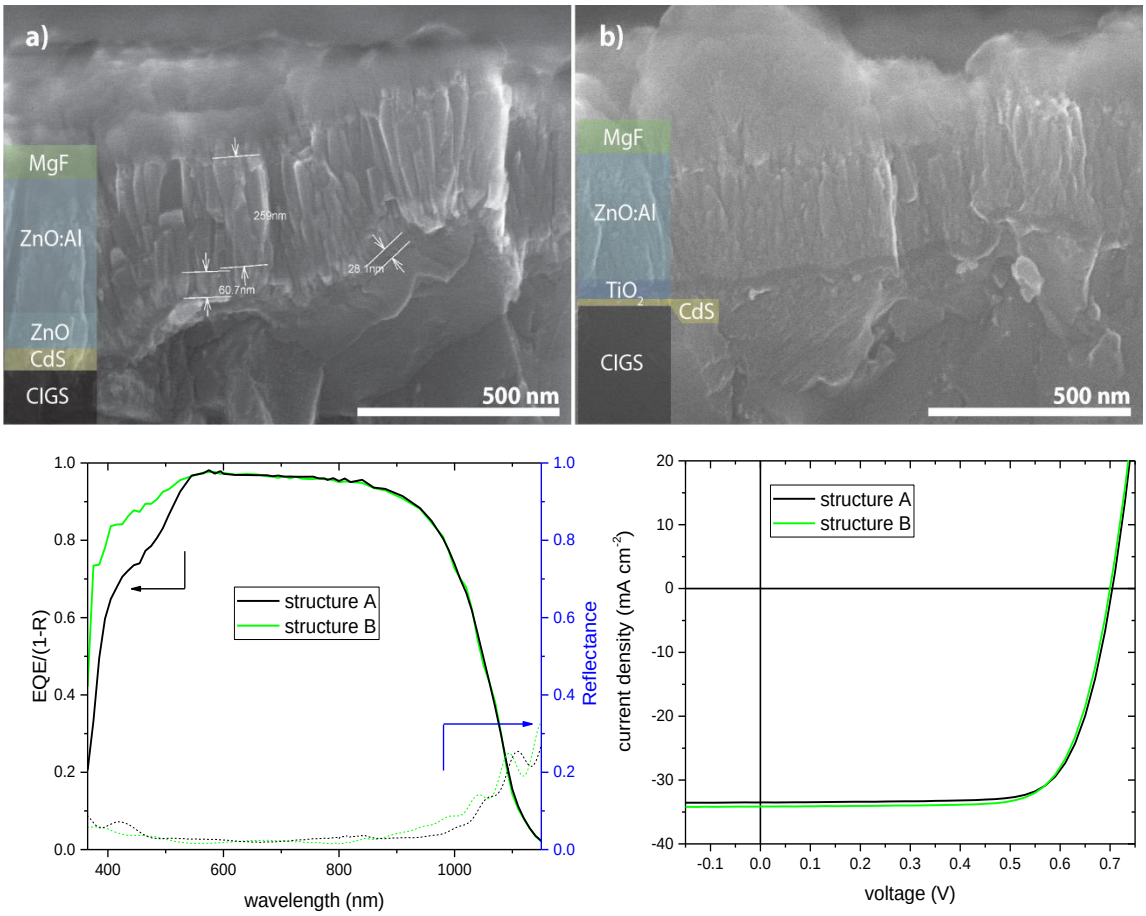

Figure 14: top: SEM micrographs of CIGS devices comprising a) 30 nm CdS / 60 nm ZnO b) 10 nm CdS / 20 nm TiO_2 as buffer layer. bottom: EQE and IV characteristics of the structures (a, b) shown above. A higher current density with structure B was obtained, with an inferior FF when compared to the reference structure A.

2.3 Task 3 Installation of an ALD setup and process development

2.3.1 Evaluation and installation of an ALD system:

After decision on the most relevant passivation layer candidates (Al_2O_3, HfO_2, Si_xN_y, SiO_2) system specifications for a deposition tool were defined. Most importantly the system should allow atomic layer deposition from gas, liquid and solid precursors. A plasma enhanced operation is also essential in order to guarantee high quality layer growth at low substrate temperature. After a public tender and evaluation period it was decided to acquire a plasma enhanced atomic layer deposition (PEALD) tool from Ultratech, MA, USA (*Figure **15***). Recipes for the relevant dielectrics were established with emphasis on growth characteristics on temperature sensitive and rough CIGS surfaces.

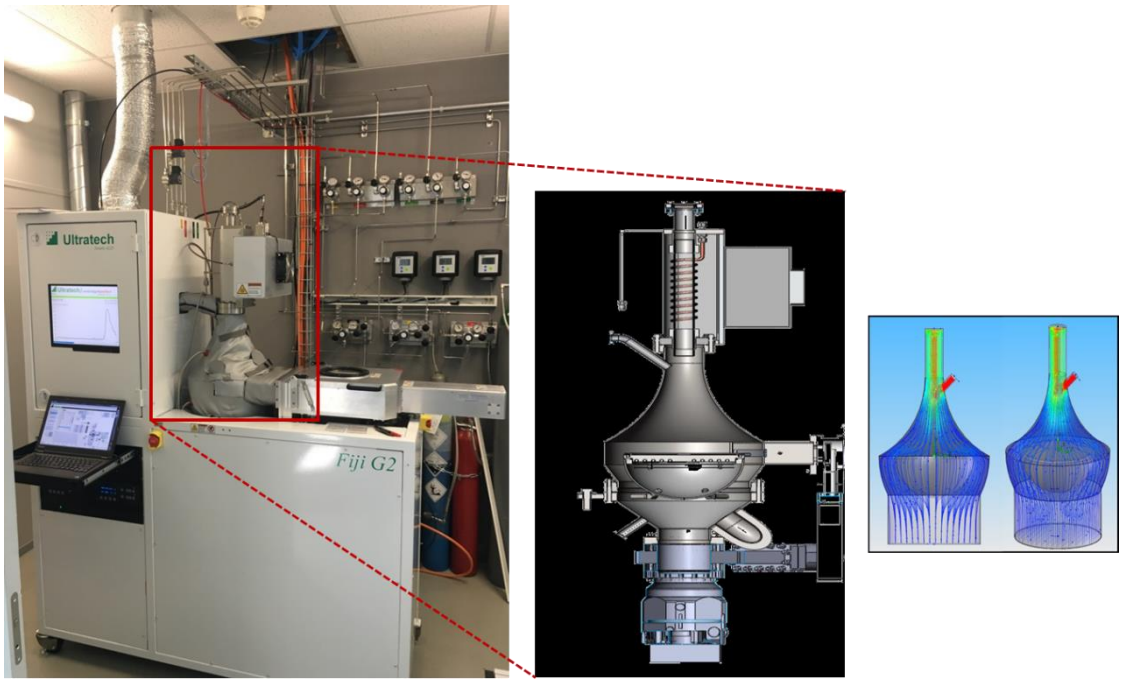

Figure 15: ALD setup, Fiji G2 by Ultratech. Right: schematics of reactor.

2.3.2 Development of metal oxide processes for surface passivation

For Al_2O_3, HfO_2 and TiO_2 deposition recipes were developed and their use as passivation layers was evaluated. TEM and SEM studies showed homogeneous layer coverage and a linear growth regime in the evaluated temperature ranges. The precursors used for the ALD deposition were chosen to allow for low temperature depositions and to have unreactive byproducts. Trimethylaluminium (TMA), tetrakis(dimethylamido)hafnium (TDMAH) and tetrakis(dimethylamido)titanium (TDMAT) with H_2O as reactant were found to be suitable precursors. The growth rate on Si (100) substrates for various deposition temperatures were investigated by ellipsometry. For Al_2O_3 a deposition temperature range from 333 – 493 K and for HfO_2 from 373 – 493 K led to a growth per cycle (gpc) of 0.078 – 0.11 nm c^{-1} (Al_2O_3) and 0.10 – 0.13 nm c^{-1} (HfO_2) respectively, with the higher growth rates for lower temperatures. Due to surface roughness, ellipsometry could not be applied to determine the growth rates directly on CIGS layers. Transmission electron microscope (TEM) study was used instead to determine the thickness and crystallinity of Al_2O_3 and HfO_2 on CIGS grown at temperatures ranging from 423 to 493 K (***Figure 16***). Some ambiguity in thickness determination comes due to a blurred contrast to the

interface of the oxide layer with the sputtered Pt coating. Still, the deposited oxide layer thickness was comparable for both the Si and CIGS substrate, but with a much larger deviation from the average for layers on CIGS. Therefore, no clear trend for the growth rate of Al_2O_3 and HfO_2 on CIGS with increasing temperature could be resolved.

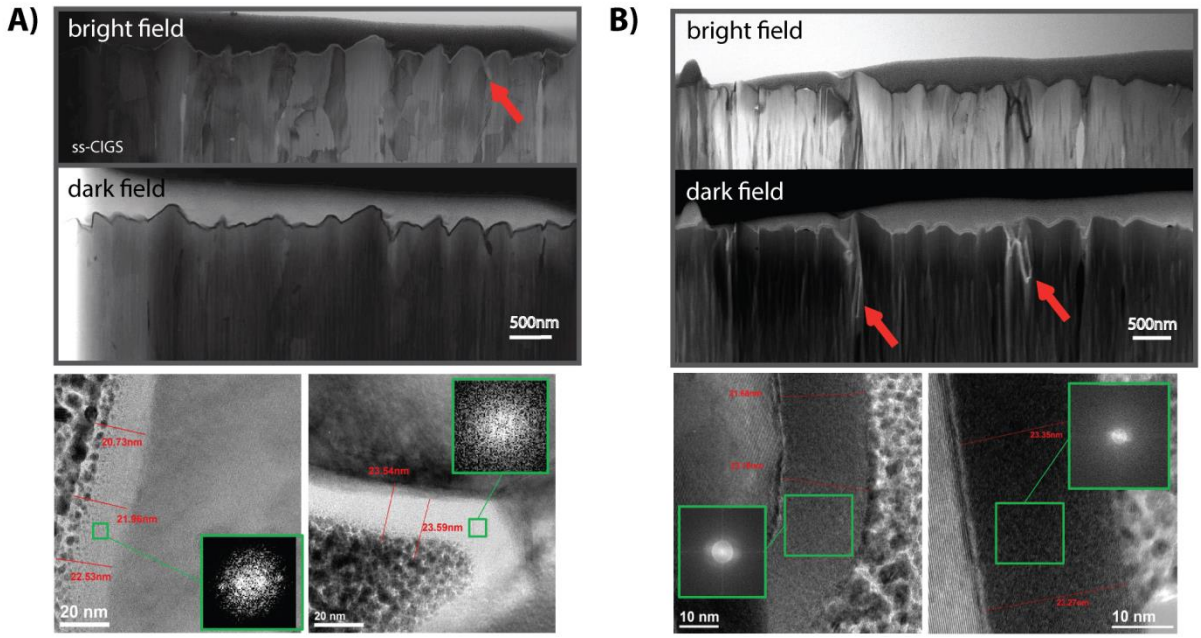

Figure 16: Top: STEM (bright field and dark field images), red arrows indicate crevices in the CIGS layer covered by the oxide; Bottom: TEM and FFT (green box inset) (2 arbitrary spots for each oxide) of aluminum oxide (A) and hafnium oxide (B) on ungraded CIGS. The coverage of CIGS by ALD is homogeneous. The oxide layers are amorphous with a few partial crystalline areas. No beam-induced crystallization was observed.

2.4 Task 4: Development of a more robust CIGS deposition process

These findings (optimized Se flux, increased absorber layer thickness, higher CGI and adjusted PDT) were implemented in the baseline process improving the cell efficiency close to 20% without antireflective coating. Champion devices reach up to 20.6%. *Figure **17*** shows the progress of the baseline process for the past 1.5 years with average cell efficiencies per substrate on either glass (triangles) or flexible polyimide (circles) substrate. It can be clearly seen that a heavy alkali PDT (NaF+RbF) shows a beneficial effect on the cell performance.

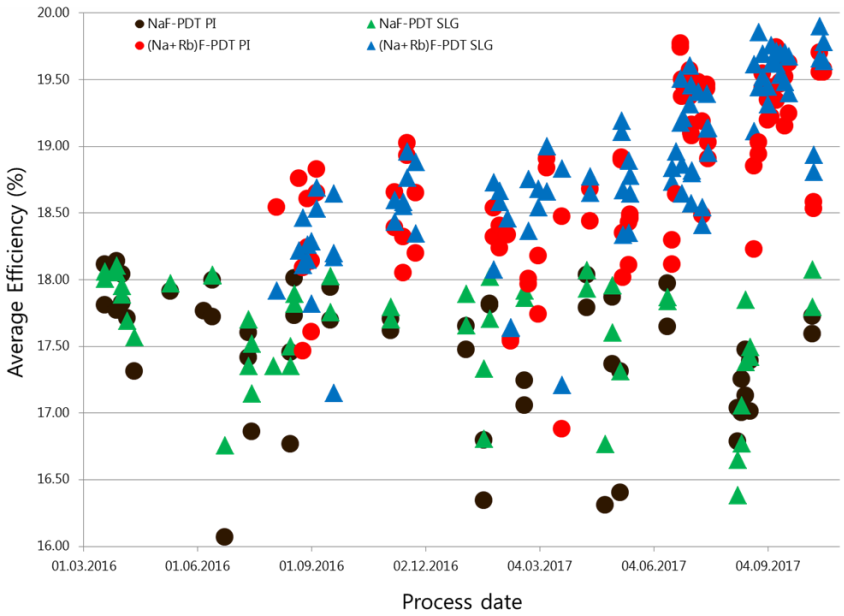

Figure 17: Average cell efficiencies of CIGS devices with alkali PDT on glass or PI substrate. The higher efficiencies and narrower distribution are obtained with heavy alkaline post deposition (RbF+NaF) treatment.

3 Conclusion

The aims of this project were the development of novel strategies to improve the photovoltaic parameters in CIGS solar cells towards 25% power conversion efficiency. Approaches to achieve this goal were to improve both the current density, by enhancing the quantum efficiency especially in the region from 700-1100 nm and reducing the current losses in the buffer layer, and the Voc by investigating methods for surface/interface passivation thus reducing carrier recombination. Combining the strategies should ultimately lead to a reproducible and high efficiency baseline process.

Equipment for the application and characterization of surface passivation layers and treatments were installed and tested. Oxide layers were deposited on CIGS by ALD and their influence on the surface recombination was investigated using TRPL. The objective of this setup was to quantify surface/interface recombination and mitigate its influence on the photovoltaic performance. A significant improvement of the luminescent decay time, i.e. reduced recombination, over the bare CIGS surface was found. This showed that the ALD-oxides Al_2O_3 and HfO_2 are indeed reducing the surface recombination rate of the CIGS/air interface which is also validated for EBIC measurements. For application in solar cells a structuring of the highly resistive oxides is necessary and an easy-to-apply scheme for structuring, which is intrinsic to the alkali PDT, was evaluated. This structuring approach was shown to be limited to a few nm of oxide thickness and hence not practicable for the requirements that TRPL measurements suggest for the oxides.

To tackle the second objective of improving the current density in the blue wavelength region Zn(O,S) was tested as an alternative buffer layer replacing CdS. A gain in current density stemming from improved quantum efficiency from 350-550 nm was achieved. Metastable light soaking effects and a reduced Voc limited the performance compared to the reference case with a CdS buffer. A different approach was taken with reducing the CdS buffer layer thickness, hence reducing its parasitic absorption, and applying TiO_2 deposited by ALD as transparent and resistive layer substituting the unintentionally doped ZnO. Again the expected gain in Jsc was observed, however, the efficiency did not improve yet due to the lower FF observed in the I-V characteristics, which is related to TiO_2.

EBIC measurements on surface-passivated CIGS cross-sections were performed in order to understand the origin of the losses in the near infrared. With these measurements insufficient absorption was identified as main loss mechanism and collection related losses can be excluded for CIGS solar cells with graded band gap. Different strategies to increase the optical absorption in the NIR included evaluated and gain in Jsc was achieved by increasing the width of the GGI notch and absorber thickness. Further, it was found that by increasing the overall copper content in the absorber a steeper absorption behavior close to the band gap is observed which leads to an improved NIR-EQE. This was achieved by investigations on the influence of the Se flux during the CIGS evaporation, the GGI grading and the CGI composition. The stepwise integration of these findings led to a steady efficiency increase of the baseline process. An average cell efficiency of about 20% was achieved.

4 Outlook

The record efficiency predicted at 22% has not been achieved so far due to inverse dependencies of solar cell parameters the new strategies or device configurations caused. Reducing the parasitic absorption of the CdS buffer layer with an alternative buffer improved, as predicted, the Jsc but simultaneously reduced Voc and FF. This limitations need to be understood and minimized in order to further improve the cell performance. The combination of a reduced CdS layer with an alternative window layer (e.g. ZnMgO) should be further investigated. Additional improvements of the NIR optical response are expected by a fine-tuning of the Ga profile and absorber composition. In order to reach 25% power conversion efficiency, further improvements of Voc and FF are paramount. This could be achieved by an increase in carrier density and life time in the absorber, an optimized band bending at the pn-junction, hence CIGS/buffer and buffer/window band alignment and reduced bulk and interface recombination rates. For this better structuring methods for highly resistive passivation layers need to be tested that are scalable and not harmful for the CIGS surface.

5 References

1. Reinhard, P., et al., *Alkali-Templated Surface Nanopatterning of Chalcogenide Thin Films: A Novel Approach Toward Solar Cells with Enhanced Efficiency.* Nano Letters, 2015. **15**(5): p. 3334-3340.
2. Jackson, P., et al., *Effects of heavy alkali elements in Cu(In,Ga)Se-2 solar cells with efficiencies up to 22.6%*,Phys. Status Solidi-R, 2016. 10: p. 583-586.
3. Mansfield, L.M., et al., *Enhanced Performance in Cu(In,Ga)Se-2 Solar Cells Fabricated by the Two-Step Selenization Process With a Potassium Fluoride Postdeposition Treatment.* Ieee Journal of Photovoltaics, 2014. **4**(6): p. 1650-1654.
4. al., D.H.e., *CIGS module manufacturing with high deposition rates and efficiencies*, in *40th IEEE Photovoltaic Spec. Conf.*2014: Denver, CO, USA.
5. Jackson, P., et al., *Compositional investigation of potassium doped Cu(In,Ga)Se-2 solar cells with efficiencies up to 20.8%.* Physica Status Solidi-Rapid Research Letters, 2014. **8**(3): p. 219-222.
6. Pianezzi, F., et al., *Unveiling the effects of post-deposition treatment with different alkaline elements on the electronic properties of CIGS thin film solar cells.* Physical Chemistry Chemical Physics, 2014. **16**(19): p. 8843-8851.
7. Handick, E., *Potassium post-deposition treatment-induced band gap widening at CIGS surfaces - Reason for performance leap?* Acs Applied Materials & Interfaces, 2015.
8. Pistor, P., et al., *Experimental indication for band gap widening of chalcopyrite solar cell absorbers after potassium fluoride treatment.* Applied Physics Letters, 2014. **105**(6).

9. Reinhard, P., et al., *Features of KF and NaF Postdeposition Treatments of Cu(In,Ga)Se-2 Absorbers for High Efficiency Thin Film Solar Cells.* Chemistry of Materials, 2015. **27**(16): p. 5755-5764.
10. Schmidt, J., et al., *Surface passivation of high-efficiency silicon solar cells by atomic-layer-deposited Al2O3.* Progress in Photovoltaics, 2008. **16**(6): p. 461-466.
11. Feldmann, F., et al., *Carrier-selective contacts for Si solar cells.* Applied Physics Letters, 2014. **104**(18).
12. Vermang, B., et al., *Introduction of Si PERC Rear Contacting Design to Boost Efficiency of Cu(In,Ga)Se-2 Solar Cells.* Ieee Journal of Photovoltaics, 2014. **4**(6): p. 1644-1649.
13. Bissig, B., et al., *Surface Passivation for Reliable Measurement of Bulk Electronic Properties of Heterojunction Devices*. Small, 2016. 12: p. 5339–5346.
14. Nishiwaki, S., et al., *Precise Se-flux control and its effect on Cu(In,Ga)Se2 absorber layer deposited at low substrate temperature by multi stage co-evaporation*, Thin Solid Films, 2017 633, p. 18–22.
15. Avancini, E., et al., *Impact of compositional grading and overall Cu deficiency on the nearinfrared response in Cu(In, Ga)Se2 solar cells* Prog. Photovolt: Res. Appl. 2017; **25**, p: 233–241.
16. Löckinger, J., et al. *New sulphide precursors for Zn(O,S) buffer layers in Cu(In,Ga)Se2 solar cells for faster reaction kinetics*. Journal of Optics, 2016 18, 084002.
17. Carron, R. et al., *Refractive Indices of Layers and Optical Simulations of Cu(In,Ga)Se2 Solar Cells*. Science and Technology of Advanced Materials 2017, submitted.